Design Analysis of SMPM Motors Using Space Fourier Transform

2.1 Introduction

A detailed literature survey on the design analysis of PM machines has been discussed in Chapter 1. This chapter deals with the merits and demerits of the methods present for the analysis of the SMPM machines and introduces the proposed method for analysis of SMPM machines as discussed in Section 2.2 and Section 2.3 respectively. The governing field equations involved and assumptions made have been discussed. Section 2.4 discusses the implementation of proposed method to AFPM motor. Calculation of the back-EMF for the SMPM motors from proposed method has been discussed in Section 2.5. The model for the calculation of cogging torque has been explained in section 2.6. Finally the chapter has been concluded in Section 2.7.

2.2 Selection of Method for Analysis for SMPM Machines

The numerical methods-FEM & BEM are powerful modern techniques and have been in trend adopted by industries and academia. However, these methods are normally not considered suitable for the initial design and optimization of electrical machines due to large computational time [Amrhein *et al.,* 2007]. Alternatively analytical lumped parameter methods like d-q-0 model and MEC [Abbaszadeh *et al.,* 2013, Virtic *et al.,* 2009] can be used for performance calculation of PM motors with certain tolerance. The necessity of modeling PM machine; and respective merits and demerits of the various methods presented has already been highlighted in Section 1.3. Analytical methods provide an insight into the effect of different design parameters and related performance of electrical machines and play a

significant role in calculating torque, back-EMF waveform prediction, cogging torque, etc., [Rahideh *et al.,* 2012a]. Though Fourier series is a widely used approach for the analysis of PM machines and provides accurate information of field distribution in the PM motors but its computational time is expected to be higher for higher speeds owing to the significant terms at higher order of space harmonics. Table 2.1 gives a comparison of the analytical methods on their capability to compute the different parameters.

The application of Fourier Transform for the design analysis of PM machines is entirely new. The method has been in use for the performance calculation of electrical machines since 1962. Some important contributions to the theory are summarized chronologically as:

i. In 1962, Fourier Transform was first introduced for determining performance of MHD generator [Fanucci *et al.,* 1962].
ii. In 1963, Sudan modified the analysis of an induction MHD generator using finite length of conducting sheet with infinite length of stator iron [Sudan *et al.,* 1963].
iii. In 1972, Yamamura described the Fourier Transform in detail for application in linear induction motors. The author discussed the effect of entry and exit end effects on the performance of LIM using both two-dimensional and three-dimensional analysis. Magnetic vector potentials (MVP) is used to predict fields and performance of the single sided and double sided LIM [Yamamura *et al.,* 1972].
iv. The method by Yamamura has been extended in 1973 for study of end-effect double-sided short stator type [Iwamoto *et al.,* 1973].
v. The effect of finite iron length and discrete windings on the performance of LIM has been studied using Fourier Transform technique [Dukowicz, 1977].

vi. Later in 1978, spatial Fourier transform .i.e., Parseval's method was used for predicting effect of transverse edge-effects in LIM [Freeman *et al.,* 1978].

vii. In 1979, a quasi 3-dimensional mathematical modeling of LIM using Fourier Transform has been presented [Lee, 1979].

viii. In 2000, Fourier transform theory has been developed for the analysis of drag plate single sided LIM considering the saturation and skin effects in the back iron [Srivastava *et al.,* 2000].

ix. The Fourier Transform has also been used to compute the effect of DC dynamic braking in LIM [Pai, 2007].

x. The performance of eddy-current brake using the same theory is reported [Srivastava *et al.,* 2009].

Conventional method uses general design equations of the machine for the calculation of output power, torque and efficiency. These methods rely on the experimental results obtained from the test body. Not suited for the performance prediction of new motor types and is useful for analyzing small changes to existing industrial designs.

Table 2.1 Comparison of Analytical methods

Parameters	MEC	Conventional method	dq0 model	Fourier series	Fourier Transform
Magnetic field	Yes	No	No	Yes	Yes
Torque	Yes	Yes	Yes	Yes	Yes
Simulation time	Large	Less	Less	Dependent on speed	Independent of speed
Expertise level	High	Low	Intermediate	High	Intermediate
Torque Vs Speed	No	Yes	Yes	No	Yes
Current Vs Speed	No	Yes	Yes	No	Yes
Computation of cogging torque	Yes	No	No	Yes	Yes

2.3 Proposed Analytical Method for SMPM Motors

The main objective of this thesis is to propose and study feasibility of proposed analytical method for design analysis of the SMPM motor. The proposed method is expected to be simple and less time consuming as compared to other methods of

analysis. SMPM motor consists of a stator with primary winding and PMs on surface of the rotor. In PMBL machines, the stator currents are in synchronism with the instantaneous rotor position, thus these machines are referred to as synchronous machines. In present approach, the SMPM machine is represented as a two-dimensional (2-D) multilayer model divided into four regions; the rotor iron, the PMs on the rotor, the air clearance or '*entrefer*' between the stator iron surface and rotor iron surface and stator yoke. In other words, the proposed 2-D analytical model defines characteristics equations in x-y plane. Each region is replaced by a homogeneous layer of respective materials having equivalent properties. For linear 2-D model, end effects are ignored. The problem is therefore simplified to a 2-D case due to the motor symmetry along its shaft. The two sources of excitation are primary stator windings and the surface mounted PMs. The present method assumes that the two sources be replaced by their equivalent current sheets.

2.3.1 Representation of Primary Stator Winding

In electromagnetic field theory, the winding currents are usually represented as current sheets. Though, the winding currents are discrete quantities with the conductors located in the slots, the current sheet is a continuous quantity. However, they are equivalent to each other if they produce same MMF as the fundamental component of their Fourier expansion. In PM machines excited by sinusoidal voltage source, the current is non-sinusoidal and contains mostly third or fifth order harmonics. The actual current flowing in one of the phase of stator windings can be given as [Yamamura *et al.*],

$$i_1 = \sum_q \sqrt{2} I_1 \exp\left(jq\omega t\right) \tag{2.1}$$

The MMF produced by the primary winding is,

$$\mathrm{MMF} = \sum_{n}\sum_{q} \frac{m\sqrt{2}}{\pi} \frac{N_1 k_w I_1}{p} \exp\left(j\left(q\omega t - nkx - \frac{\pi}{2} \right) \right) \tag{2.2}$$

The equivalent current density sheet for the above primary current is given by,

$$j_1 = \sum_{n}\sum_{q} \sqrt{2} J_1 \exp\left(j\left(q\omega t - nkx \right) \right) \tag{2.3}$$

k is given by,

$$k = \frac{\pi}{\tau} \tag{2.4}$$

Hence,

$$J_1 = \frac{m\sqrt{2}}{\pi} \frac{N_1 k_w I_1}{p\tau} \text{ A/m} \tag{2.5}$$

2.3.2 Representation of Permanent Magnets

The PMs may be modeled as equivalent flux source, equivalent current sheet, by an MMF source or by a Magnetization vector. N. Boules in his work presented PMs as surface current density [Amrhein *et al.,* 2007].The equivalent MMF produced by the PMs can be written as [Deng *et al*., 1986],

$$\mathrm{MMF}_p = H_c h_m \tag{2.6}$$

When modeled as a flux source as in MEC method, the value of the flux source depends on the reluctance and coercivity of PM and is equal to [Ghalavand *et al.*, 2010],

$$\varphi_p = \frac{H_c h_m}{\Re_m} \tag{2.7}$$

With PMs of alternate polarities are present on the rotor, the magnetization vector in the Fourier Series as shown in Fig. 2.1 can be written as [Boroujeini *et al.*, 2009],

$$\mathbf{M}_y = \sum_{n=1,3,....} \frac{4B_r}{n\pi\mu_0} \sin\left(\frac{n\pi\alpha}{2}\right)\cos\left(\frac{n\pi y}{\tau}\right) \tag{2.8}$$

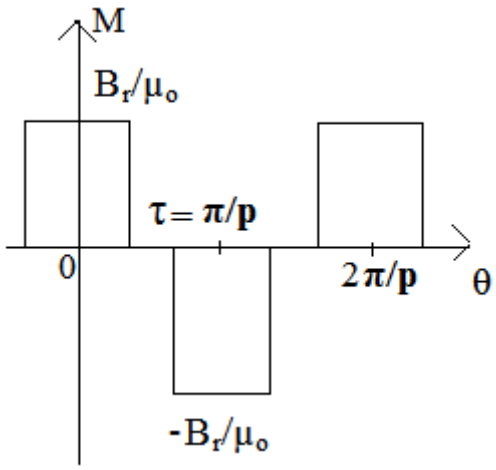

Fig. 2.1 Distribution of Magnetization of Permanent Magnets

The PMs produces a constant field in the air gap as DC field winding. The DC excitation has been represented by equivalent sheet [Shanmugasundaram *et al*., 1983]. In the similar manner, the PMs may also be represented by equivalent current density and is given as,

$$j_2(x) = \sum_{n} J_2 \, exp\, j(q\omega t - nk_2 x \pm \phi) \text{ A/m} \tag{2.9}$$

where,

$$J_2 = \frac{H_c h_m}{\tau_m} \tag{2.10}$$

Equation (2.9) produces the same MMF as the equation (2.8) and hence the PMs can be represented by their equivalent current sheet.

The general assumptions made for the proposed analysis are:

2.3.3 Assumptions

a. For isotropic model, the stator iron is assumed to have infinite permeability, thus neglecting magnetic saturation of the core.

b. The current flows only in z-direction.

c. The stator is laminated, thus the eddy currents in stator are ignored.

d. The electromagnetic properties of all materials are linear, isotropic and temperature invariant.

e. The two current sheets are present over a length of x=0 to x=L, where L=peripheral length of motor bore for solution in real space.

f. The flux density vector has only radial and tangential component, thus magnetic vector potential has only z-component.

g. The slotting effect has been taken into account using Carter's coefficient.

h. For anisotropic model, the stator is assumed to have multiple layers and stator yoke is assumed to have infinite permeability. While the proposed model takes care of saturation in the stator core which is valid for machine with lesser *entrefer*.

i. The presence of slots and their effect on average air clearance is taken into account using Carter's coefficient. Slotting in the stator reduces flux per pole in the air gap and thereby reduces average torque of the motor. The effective air gap or *'entrefer'* corrected by Carter's coefficient as,

$$g_e = g + (k_c - 1)\, g' \tag{2.11}$$

where Carter's coefficient k_c is given by [Zhu *et al*., 1993a],

$$k_c = \frac{\tau_t}{\tau_t - \gamma g'} \tag{2.12}$$

$$g' = g + \frac{h_m}{\mu_r} \tag{2.13}$$

$$\gamma = \frac{4}{\pi}\left\{\frac{w_0}{2g'}\tan^{-1}\left(\frac{w_0}{2g'}\right) - \ln\sqrt{1+\left(\frac{w_0}{2g'}\right)^2}\right\} \tag{2.14}$$

Fig. 2.2 shows a typical outer rotor 12-slot 2-pole SMPM motor. The proposed analysis has been reported for cases without stator slotting .i.e., isotropic model and with the effect of slotting .i.e., anisotropic model. The permeability of stator yoke has been assumed to be infinity whereas the relative permeability of PMs is assumed close to unity. Rare-earth PMs have linear second quadrant characteristics with recoil permeability nearly equal to air gap permeability μ_o so that they can stand severe demagnetization and magnetization cycles due to high armature reaction fields [Deng *et al.,* 1986]. The proposed analytical model of the SMPM motors has been shown in Fig. 2.3 while the simplified linear model of the SMPM motor is shown in Fig 2.4 (a) and (b). The problem is simplified to two-dimensional case due to symmetry along motor shaft. Initially, the regions are considered to be isotropic, however the slotting effect is included in an anisotropic model. The layer representing the magnets is assumed to have average conductivity and average permeability and slotted stator structure is replaced by a smooth core as in Fig. 2.5 (a) and (b). Current sheets substituting the primary windings and layer of permanent magnets are present on the surface of stator core and PM layer respectively. These are assumed to be infinitesimally thin. The rotor permanent magnets will be aligned with the crust of stator rotating magnetic field, giving maximum normal force or no tangential force when space angle is φ=0° or φ=180°. The primary coils of stator are switched ON and OFF in synchronism with the rotor instantaneous position. The PM rotor follows the rotating magnetic field created by the stator winding currents. The magnetic rotor under

steady state conditions runs at exact synchronous speed. It has been shown in equation (2.24) that when rotor peripheral speed is equal to synchronous speed $v=v_s=2\tau f$, the displacement angle is φ=90°, or in other words the spatial phase difference between two current sheets is φ=±j0.5kτ.

The magnetic field H around a small path enclosing the two current sheets $j_1(x)$ and $j_2(x)$ located along x is,

$$g\frac{\partial H}{\partial x} = j_1 + j_2 \tag{2.15}$$

In the air gap,

$$B=\mu_o H \tag{2.16}$$

therefore,

$$\frac{\partial \mathbf{B}}{\partial x} = \frac{\mu_o}{g}\left(j_1 + j_2\right) \tag{2.17}$$

The line integral of electromotive force induced can be written as,

$$\frac{\partial e_2}{\partial x} = \frac{\partial B}{\partial t} + v\frac{\partial B}{\partial x} \tag{2.18}$$

Since the secondary sheet is assumed to have no leakage inductance, the EMF induced in secondary will be considered as resistance drop,

$$e_2 = \rho_s j_2 \tag{2.19}$$

From equation (2.16), (2.17) and (2.18),

$$\frac{g}{\mu_0}\frac{\partial^2 B}{\partial x^2} - \frac{v}{\rho_s}\frac{\partial b}{\partial x} - \frac{1}{\rho_s}\frac{\partial b}{\partial t} = \frac{\partial j_1}{\partial x} \tag{2.20}$$

The steady state solution of equation (2.20) is given by,

$$B_s = B_0 \exp\left\{ j\left(\frac{\pi}{\tau} v_s t - \frac{\pi}{\tau} x \pm \varphi \right) \right\} \tag{2.21}$$

where,

$$B_o = \frac{J_1}{\sqrt{\left(\frac{\pi g}{\tau \mu_0}\right)^2 + \left[\frac{1}{\rho_s}(v_s - v)\right]^2}} \tag{2.22}$$

and

$$\varphi = \pm \tan^{-1} \frac{\pi \rho_s g}{\mu_o \tau (v_s - v)} \tag{2.23}$$

thus, when $v_s = v$ $\varphi = \pm 90°$ (2.24)

The variation of torque at different displacement angles has been shown in Fig 2.6. It can be depicted that the maximum torque occurs at 90°. Here '±' sign indicates the direction of rotation.

2.3.4 Governing Field Equations

Maxwell's field equations are used to derive the governing partial differential equations. The basic equations involved are,

$$\nabla . \mathbf{D} = \rho \tag{2.25}$$

$$\nabla . \mathbf{B} = 0 \tag{2.26}$$

$$\nabla \mathrm{x} \mathbf{H} = \mathbf{J} \tag{2.27}$$

The general governing field Maxwell's equations for PMBLAC motor having conducting material on rotor is,

$$\nabla^2 \mathbf{A} = -\mu_0 \left(\mathbf{J} + \nabla \times \mathbf{M} + \mathbf{J}_t + \mathbf{J}_\upsilon \right) \tag{2.28}$$

where, J is the source current density of current carrying conductors of primary replaced by linear current density J_p, J_t is transformer eddy current density in moving conducting media, J_v is speed induced current density in moving conducting media and $\nabla \times \mathbf{M}$ is the MMF due to magnets replaced by linear current density J_s.

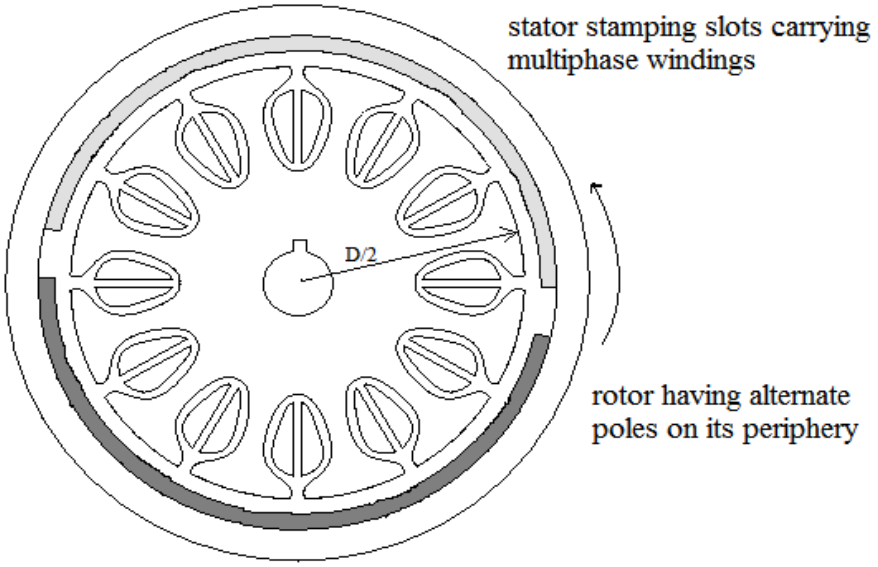

Fig 2.2 A Typical 12-slot Surface Mounted PM motor *(windings not shown for clarity)*

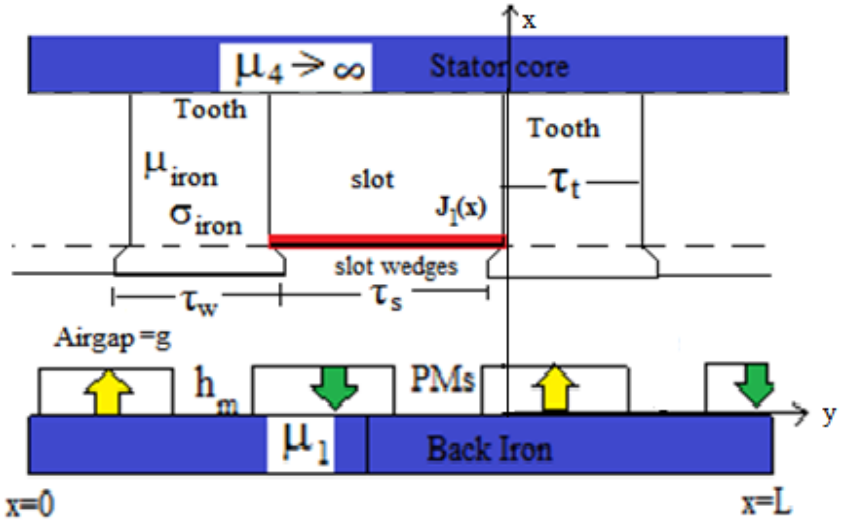

(a)

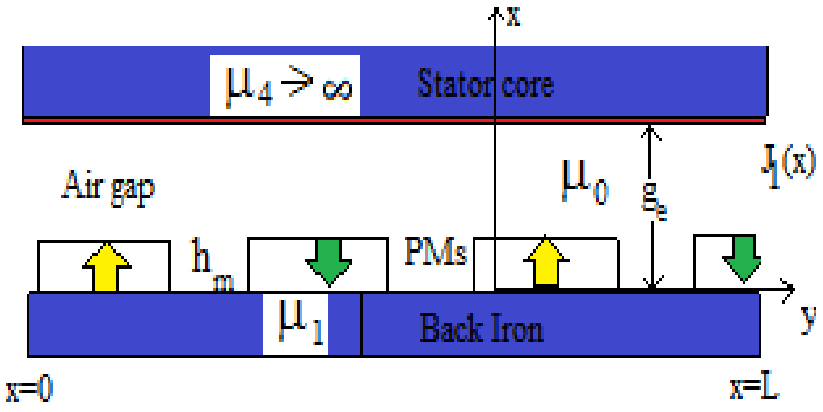

(b)

Fig. 2.3 Linear Model of PM motor (a) with slots and PMs (b) slots neglected

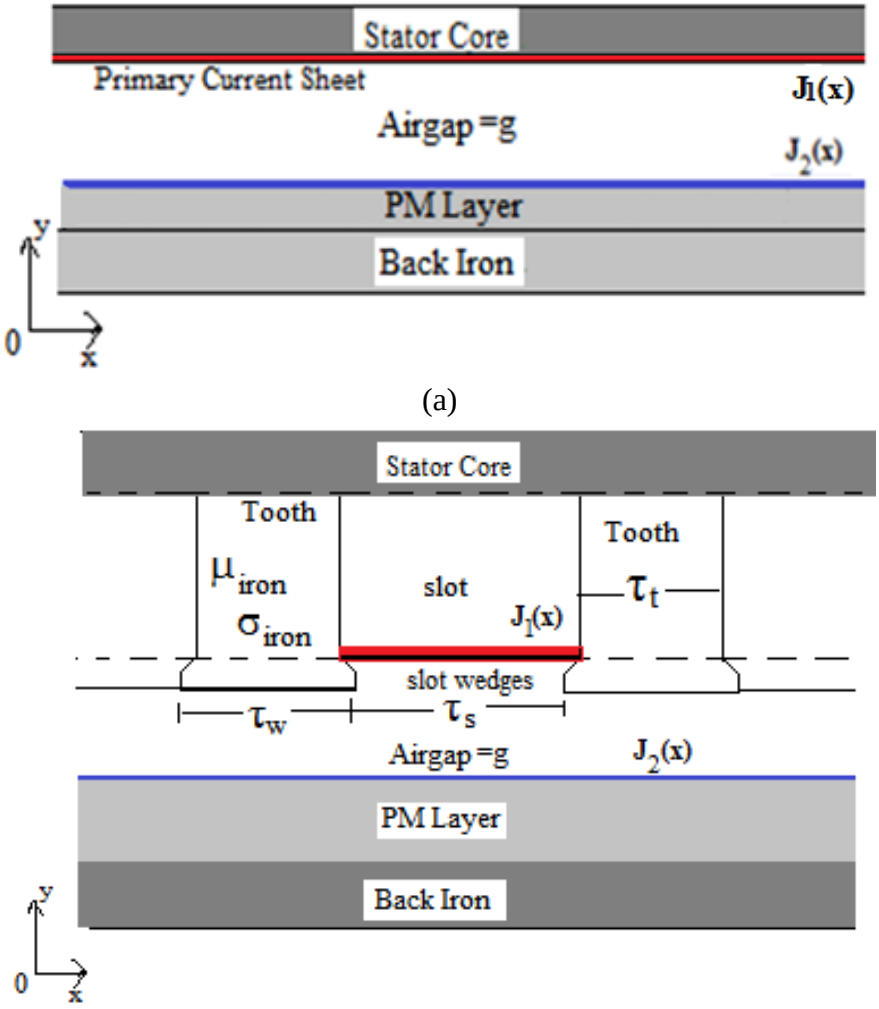

Fig. 2.4 Simplified Linear Model of the Surface Mounted PM Machine (a) Isotropic (b) Anisotropic

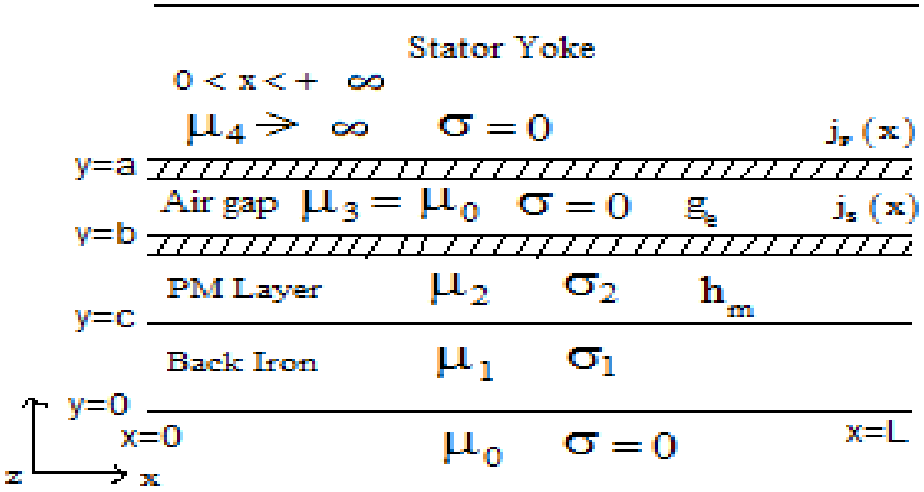

(a)

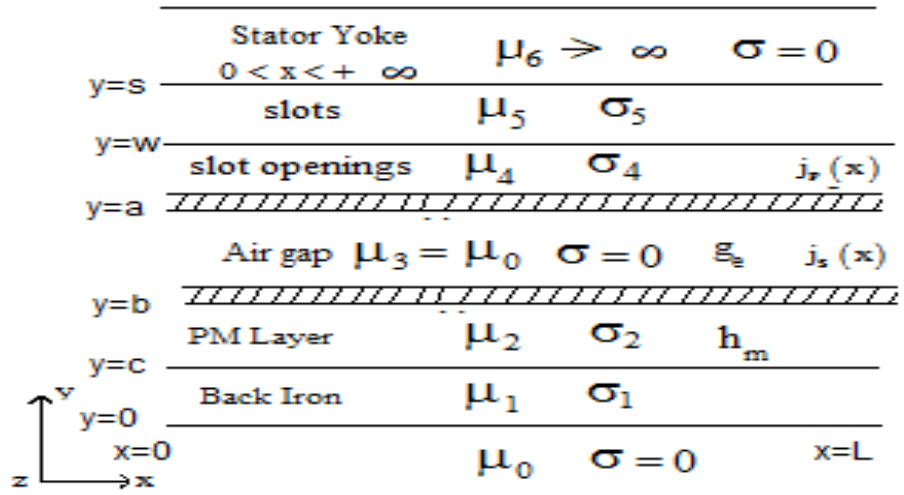

(b)

Fig 2.5 Typical layer models of PMBL motor- (a) Isotropic model- stator winding is replaced by linear current density j_P (x) and PM layer are represented by linear current density j_S (x) (b) Anisotropic layer model of PMBL motor taking slots and slot openings into account. (Current sheets are assumed to be infinitesimally thin)

For PMs,

$$\mathbf{B}=\mu_0\mu_r\mathbf{H}+\mu_0\mathbf{M} \tag{2.29}$$

For regions other than PMs,

$$\mathbf{B}=\mu_0\mu_r\mathbf{H} \tag{2.30}$$

$$\nabla x\mathbf{B}=\mu_0\nabla x\mathbf{M} \tag{2.31}$$

Magnetic vector potential can be defined as,

$$\mathbf{B}=\nabla x\mathbf{A} \tag{2.32}$$

$$\nabla x\mathbf{B}=\nabla x\nabla x\mathbf{A}=\nabla\left(\nabla.\mathbf{A}\right)-\nabla^2\mathbf{A} \tag{2.33}$$

Coulomb Gauge,

$$\nabla.\mathbf{B}=0 \tag{2.34}$$

$$\nabla x\mathbf{B}=-\nabla^2\mathbf{A} \tag{2.35}$$

$$\nabla^2\mathbf{A}=-\ \mu_o\left(\mu_r\mathbf{J}_f+\nabla x\mathbf{M}\right) \tag{2.36}$$

The governing field equations for conducting moving media having finite conductivity,

$$\nabla^2\mathbf{A}_l=\mathrm{j}\omega\mu_l\sigma_l\mathbf{A}_l-\mathrm{v}\mu_l\sigma_l\left(\frac{\partial\mathbf{A}_l}{\partial x}\right) \tag{2.37}$$

Magnetic Vector Potential (MVP) has z-component only and is denoted as A or A_z. The Fourier transform of MVP $A_z(x, y)$ is $\tilde{A}_z(\xi,y)$ and is given by,

$$\tilde{A}\left(\xi,y\right)=\int_{-\infty}^{\infty}A_z\left(x,y\right)e^{-j\xi x}dx \tag{2.38}$$

Fourier Transform is applied for the solution of Maxwell's equations for analysis of PM motors and the magnetic vector potential (MVP) of each layer is calculated separately utilizing the above boundary conditions. Since, the model has two

conducting layers presenting primary windings and PM layer, the Fourier transform of the two current sheets can be written as,

$$\tilde{\mathbf{J}}_1(\xi) = \sum_r j\left[e^{-jr(k_1+\xi)L} - 1\right]\frac{J_1}{r(\xi+k_1)} \tag{2.39}$$

$$\tilde{\mathbf{J}}_2(\xi) = \sum_n j\left[e^{-j(k_2+\xi)L} - 1\right]\frac{e^{\pm j0.5k\tau}J_2}{n(\xi+k_2)} \tag{2.40}$$

In order to establish the theory of Fourier transform applicable to PMBLAC motor, it is initially assumed that,

$$k_1 = k_2 = k = \frac{\pi}{\tau} \tag{2.41}$$

2.3.5 Boundary Conditions

1.All field components are zero at z = ±∞.

2.For interface between limiting boundary and homogeneous layer, Neumann type boundary conditions applied are,

$$\tilde{H}_{x\bar{l}}(\xi) = \tilde{H}_{x\overline{l-1}}(\xi) \tag{2.42}$$

3. For interface between homogeneous layers (conducting and non-conducting layers), continuous boundary conditions are applied as,

$$\tilde{H}_{x\bar{l}}(\xi) - \tilde{H}_{x\overline{l-1}}(\xi) = \tilde{\mathbf{J}}(\xi) \tag{2.43}$$

$$\frac{\partial \tilde{A}_l(\xi)}{\partial y} - \frac{\partial \tilde{A}_{l-1}(\xi)}{\partial y} = \mu\tilde{\mathbf{J}}_1(\xi) \tag{2.44}$$

Here, **J**(ξ) is the Fourier transform of current sheet present at the interface.

4.Magnetic vector potential : At the interface between two layers,

$$\tilde{A}_l(\xi) - \tilde{A}_{l-1}(\xi) = 0 \tag{2.45}$$

In air gap or *'entrefer'*,

$$\nabla^2 \mathbf{A} = 0 \tag{2.46}$$

and coulomb gauge is defined as,

$$\nabla . \mathbf{A} = 0 \tag{2.47}$$

For permanent magnets as per Poisson's equation,

$$\nabla^2 \mathbf{A} = -\mu_0 \nabla x \mathbf{M} \tag{2.48}$$

Assumed solutions of PMBLAC motor are given by following set of equations for isotropic model,

At 0^{th} layer,

$$\tilde{A}_o(\xi) = \tilde{A}_n(\xi) e^{\xi y} \tag{2.49}$$

and at other regions of layer model,

$$\tilde{A}_1(\xi, y) = \tilde{B}_n(\xi) e^{\chi y} + \tilde{C}_n e^{-\chi y} \tag{2.50}$$

$$\tilde{A}_2(\xi, y) = \tilde{D}_n(\xi) e^{\gamma y} + \tilde{E}_n(\xi) e^{-\gamma y} \tag{2.51}$$

$$\tilde{A}_3(\xi, y) = \tilde{F}_n(\xi) e^{\xi y} + \tilde{I}_n(\xi) e^{-\xi y} \tag{2.52}$$

$$\tilde{A}_4(\xi, y) = \tilde{P}_n(\xi) e^{\chi y} + \tilde{Q}_n(\xi) e^{-\chi y} \tag{2.53}$$

$$\tilde{A}_5(\xi, y) = \tilde{R}_n(\xi) e^{\chi y} + \tilde{S}_n(\xi) e^{-\chi y} \tag{2.54}$$

where,

For back iron, $$\chi^2 = \xi^2 + j\omega\mu_1\sigma_1 + j\xi\upsilon\mu_1\sigma_1 \tag{2.55}$$

For PMs, $$\gamma^2 = \xi^2 + j\omega\mu_2\sigma_2 + j\xi\upsilon\mu_2\sigma_2 \tag{2.56}$$

In case of anisotropic model, the slotted regions are assumed to be homogenized by anisotropic material properties. When a layer consists of two materials as in a slot, the equivalent material property takes care of the variation or change in the flux. The anisotropic magnetic permeability in the region of slot openings and slot is calculated as [Williamson, 1976],

$$\mu_{4x} = \frac{\mu_0 \mu_1 \left(\tau_s + \tau_w\right)}{\mu_1 \tau_s + \mu_0 \tau_w} \tag{2.57}$$

$$\mu_{4y} = \frac{\mu_1 \tau_w - \mu_0 \tau_s}{\tau_s + \tau_w} \tag{2.58}$$

$$\mu_{5x} = \frac{\mu_0 \mu_1 \left(\tau_c + \tau_t\right)}{\mu_1 \tau_c + \mu_0 \tau_t} \tag{2.59}$$

$$\mu_{5y} = \frac{\mu_1 \tau_t - \mu_0 \tau_c}{\tau_c + \tau_t} \tag{2.60}$$

thus in slot openings,

$$\mu_4 = \sqrt{\mu_{4x}^2 + \mu_{4y}^2} \tag{2.61}$$

and in slot regions,

$$\mu_5 = \sqrt{\mu_{5x}^2 + \mu_{5y}^2} \tag{2.62}$$

Using equations (2.40) and (2.41) and solving MVP for different regions,

$$\tilde{A}_n\left(\xi\right) = - \frac{\mu_3 \left[\tilde{\mathbf{J}}_1(\xi) + \tilde{\mathbf{J}}_2(\xi) \cosh \xi (a - b)\right]}{\xi . \tilde{K}\left(\xi\right)} \tag{2.63}$$

MVP at the air gap where current sheet is present for isotropic model is derived as,

$$\tilde{A}_3(\xi,a)=\sum_r \frac{\mu_3}{\xi}\tilde{J}_1(\xi)\frac{\tilde{W}(\xi,a)}{\tilde{K}(\xi)} \tag{2.64}$$

MVP at the interface where primary current sheet is present for anisotropic model is derived as,

$$\tilde{A}_5(\xi,a)=\sum_r \frac{\mu_5}{\chi}\tilde{J}_1(\xi)\frac{\tilde{G}(\xi,a)}{\tilde{H}(\xi)} \tag{2.65}$$

Using inverse transformation of magnetic vector potential,

$$A_3(x,y)=j\frac{\mu_3}{2\pi}J_1\int_{-\infty}^{\infty}\sum_r \frac{\left(e^{-j(\xi+k)L}-1\right)}{(\xi+k)}\frac{\tilde{W}(\xi,a)}{\tilde{K}(\xi)}e^{j\xi x}dx \tag{2.66}$$

$$A_5(x,y)=j\frac{\mu_5}{2\pi}J_1\int_{-\infty}^{\infty}\sum_r \frac{\left(e^{-j(\xi+k)L}-1\right)}{(\xi+k)}\frac{\tilde{G}(\xi,a)}{\tilde{H}(\xi)}e^{j\xi x}dx \tag{2.67}$$

The calculation of $\tilde{W}(\xi,a)$, $\tilde{K}(\xi)$, $\tilde{G}(\xi,a)$ and $\tilde{H}(\xi)$ are given in Appendix A.

2.3.6 Magnetic Field and Torque Calculation

Since, magnetic vector potential (MVP) of the proposed analytical model is 2-D in x-y plane has only z-component, therefore

$$\tilde{\mathbf{B}}_x=\frac{\partial\tilde{\mathbf{A}}_z}{\partial y} \qquad \tilde{\mathbf{B}}_y=-\frac{\partial\tilde{\mathbf{A}}_z}{\partial x} \tag{2.68}$$

The y-component of the magnetic flux density is more important as it produces torque in combined action with the primary current J_1. Now, the flux density at the air gap can be calculated as,

$$\tilde{\mathbf{B}}_{3y}(\xi,y)=-\frac{\partial\tilde{\mathbf{A}}_3(\xi,y)}{\partial x} \tag{2.69}$$

$$\tilde{\mathbf{B}}_{3y}(\xi,y) = -j\xi\tilde{\mathbf{A}}_3(\xi,y) \tag{2.70}$$

Substituting value of $\tilde{\mathbf{A}}_3(\xi,y)$ from equation (2.64) in equation (2.70),

$$\tilde{\mathbf{B}}_{3y}(\xi,y) = -\frac{\mu_3}{2\pi} J_1 k \frac{\tilde{W}(\xi,y)}{\tilde{K}(\xi)} e^{j\xi x} \tag{2.71}$$

Torque is developed between the primary current sheet present between the length x=0 to x=L= $2\pi R_o$ and permanent magnets and is given in closed form solution as,

$$T = R_o p \int_0^L \Re e\left[\tilde{\mathbf{J}}_1^*(\xi)\mathbf{B}_{3y}\right] dx \tag{2.72}$$

$\mathbf{J}_1^*$ is the complex conjugate of the $\mathbf{J}_1$.

The Fourier transform technique uses Parseval's theorem and Residue theorem for obtaining the solution in Fourier space and Real space respectively.

A. Solution Using Residue Theorem

Residue Theorem has been utilized in inverse transforming Fourier Transforms in solutions of separate variable. It is advantageous for obtaining answers of analytical solutions of separate variable. In Residue Theorem, poles of the integrand need to be calculated for linear and segmented PM machines where exit and end effects mark their presence while it is not essentially required in cylindrical PM machines.

The above integration when carried out using Residue Theorem, the poles are,

$$\xi + k = 0 \tag{2.73}$$

$$\tilde{K}(\xi) = 0 \tag{2.74}$$

Thus, from equation (2.73) is ξ=-k. In case of rotary permanent magnet motor excited by an alternating current, the pole ξ=-k is responsible for the generation of main torque. However, for the linear or segmented PM motor where entry and exit end effects are

dominant similar to that of linear induction motor, the poles responsible for generation of torque is,

$$\tilde{K}(\xi)=0 \tag{2.75}$$

The pole ξ=-k near origin on negative real axis in the complex-plane is a significant pole representing the pole pitch of primary stator winding. Fig. 2.7 shows the location of this pole in ξ-plane. Substituting ξ=-k in equation (2.64), MVP at the air gap for isotropic model is derived as,

$$\mathbf{A}_3(-k,a)=j\sum_r \frac{\mu_3}{2\pi} J_1 \frac{W(-k,a)}{K(-k)} e^{-jkx} \tag{2.76}$$

Magnetic flux density in the air gap can be calculated combining the equations (2.70) and (2.76) as,

$$\mathbf{B}_{3y}(-k,a) = -\frac{\partial \mathbf{A}_3(-k,a)}{\partial x} \tag{2.77}$$

$$\mathbf{B}_{3y}(-k,a) = -j\xi \mathbf{A}_3(-k,a) \tag{2.78}$$

Substituting value of A_{3z}(-k,a) in the equation (2.78) from equation (2.76),

$$\mathbf{B}_{3y}(-k,a) = -\frac{\mu_3}{2\pi} \mathbf{J}_1 k \frac{W(-k,a)}{K(-k)} e^{-jkx} \tag{2.79}$$

Therefore, torque developed using Residue Theorem has been computed as,

$$T=\frac{\mu_0 J_1^2 R_o p}{2} \Re e\left[\frac{jkLW(-k,a)}{K(-k)}\right] \tag{2.80}$$

The torque developed for anisotropic model can be calculated in the similar way using equation (2.66) and (2.67). ξ=-k

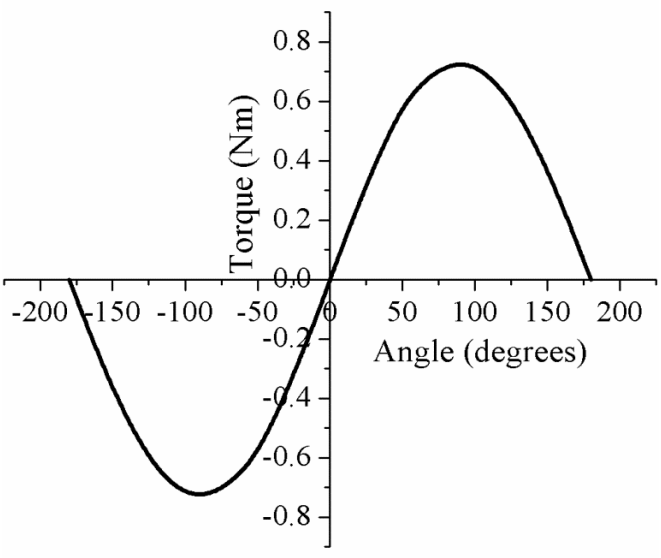

Fig 2.6 Variation of Torque with displacement angle between two current sheets

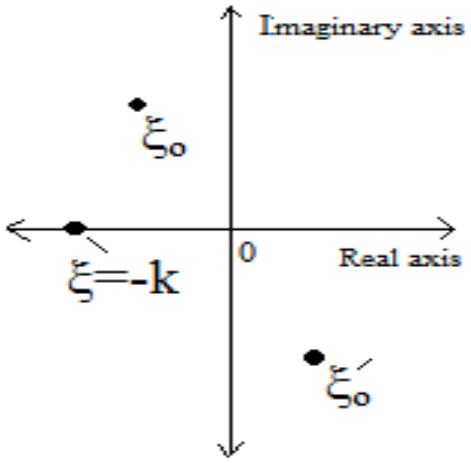

Fig. 2.7 Location of poles in the ξ-plane

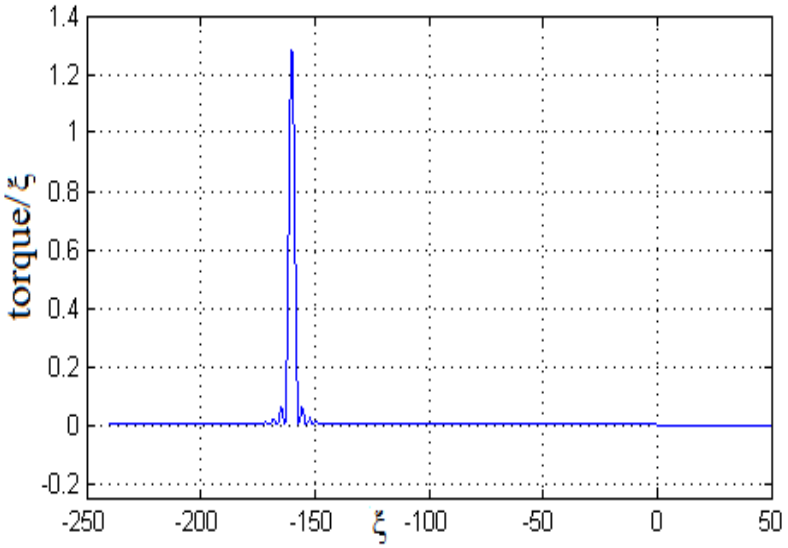

(a)

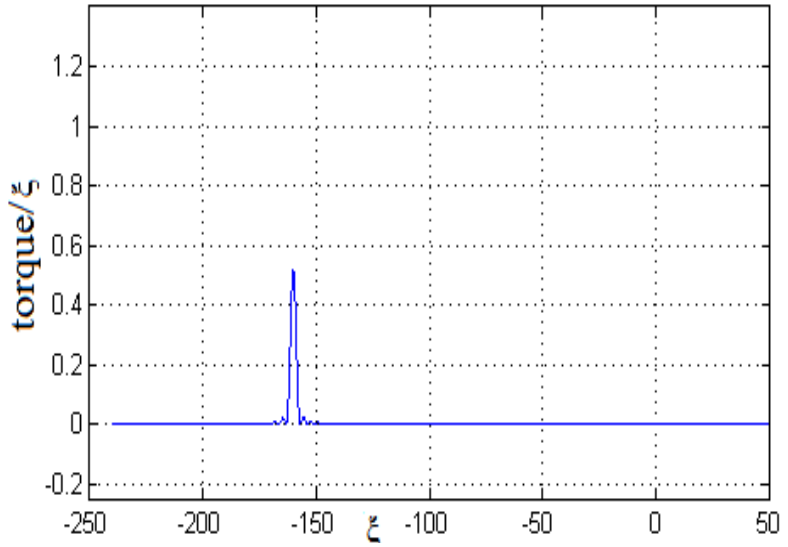

(b)

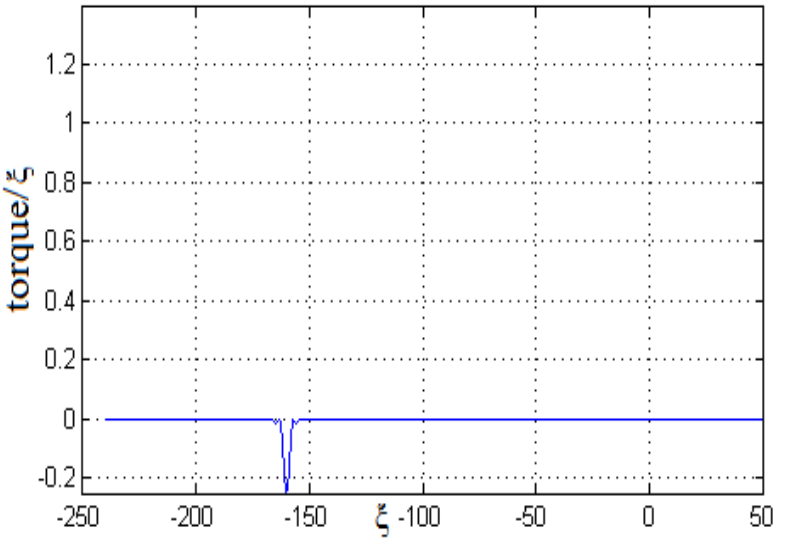

(c)

Fig. 2.8 Typical variation of torque integrands of PMBLAC motor at (a) standstill (b) 400 RPM (c) 800 RPM

When solution is obtained in real space using Residue Theorem the torque expression takes the form,

$$T=T_1\left(\xi=-k\right)+T_2\left(\xi=-\xi_0\right)+T_3\left(\xi=-\xi_0'\right) \tag{2.81}$$

For cylindrical PM machines, T_2 and T_3 both are zero. For segmented and linear PM machine ξ_0 and ξ_0' are numerically computed using equation (2.75) for different operating conditions. However, this is beyond the scope of the present work.

B. Solution using Parseval's Theorem:

Parseval's theorem is used to facilitate numerical calculation of torque and other quantities which are calculated as products of physical quantities such as voltage, flux density and current. When Fourier transforms of the physical quantities are known, the motor performances can be computed directly from Fourier Transform using Parseval's Theorem.

When $f_1(x)$ and $f_2(x)$ are limited and integral in limits ($-\infty$ to ∞),

$$\int_{-\infty}^{\infty}\tilde{f}_1^*\left(\xi\right)\tilde{f}_2\left(\xi\right)d\xi=\frac{1}{2\pi}\int_{-\infty}^{\infty}f_1^*\left(x\right)f_2\left(x\right)dx \tag{2.82}$$

Torque produced with the interaction of primary stator current and PMs,

$$T=\frac{R_o p}{2}\Re e\int_{-\infty}^{\infty}\tilde{\mathbf{J}}_1^*\left(\xi\right)\mathbf{B}_{3y}d\xi \tag{2.83}$$

$$T=\frac{R_o p}{4\pi}\Re e\int_{0}^{L}\tilde{\mathbf{J}}_1^*\left(\xi\right)\mathbf{B}_{3y}d\xi \tag{2.84}$$

$$T=\frac{R_o p}{\pi}\mu_3 J_1^2\int_0^L\frac{1-\cos\left(\xi+k\right)L}{\left(\xi+k\right)^2}\Im mag\left(\frac{\tilde{W}\left(\xi,a\right)}{\tilde{K}\left(\xi\right)}\right)d\xi \tag{2.85}$$

The torque is calculated numerically using above equation. The range of 'ξ' and step length 'dξ' both have been obtained using trial and error method, so as to cover the relevant distribution of integrands in Fourier space. The numerical integration has been performed using MATLAB software for real values of ξ = -250 to +50 at a step length of dξ = 0.1081. The general distribution of torque integrand in Fourier Space at standstill, 400 RPM and 800 RPM for a 12-slot RFPM machine whose details are given in Table 3.1 has been shown in Fig. 2.8. The torque distribution is more pronounced at ξ=-π/ τ in real axis. However Residue method gives a closed form solution and uses more realistics assumptions, the technique is expected to be better than that of Parseval's method.

2.4 Proposed Analytical Model for AFPM Motor

AFPM machines have intrinsic 3-D electromagnetic structure, however since 3-D FEM is very time consuming especially for initial design analysis and optimization, 2-D FEM and analytical methods are generally preferred for this purpose. The analytical calculations to determine the air gap flux density distribution is performed at an average radius calculated as equation (2.86). Both the methods, FEM and analytical method give accurate results however analytical methods using solution of MVP for performance analysis are faster than the FEM [Choi *et al.*, 2011].

The proposed 2-D analytical method for SMPM machines can be applied to radial flux as well as axial flux PM machines. The mean radius of the AFPM motor is,

$$R_{ave} = \frac{D_0 - D_i}{2} \tag{2.86}$$

The torque can be calculated for AFPM motor using Residue Theorem and Parseval's Theorem from equations (2.80) and (2.85) respectively with $R_o=R_{ave}$.

2.5 Back-EMF

For calculation of back-EMF, computation of no-load magnetic flux is necessary and is given as,

$$\phi_o = \frac{\alpha\pi}{2P} B_g R_1^2 \left(1 - \frac{R_2^2}{R_1^2}\right) \tag{2.87}$$

The Back-EMF induced in the primary stator windings can be calculated using,

$$EMF = \pi\sqrt{2} N_1 k_w \phi_o n_s / p \tag{2.88}$$

2.6 Cogging Torque

Cogging torque in SMPM motors arise from interactions of the PM flux and stator or rotor slots. It is a primary source of ripple in output torque which depends on the PM flux and the reluctance variation and is independent of the supply current and variation in current due to loads [Chun *et al.*, 2006]. Cogging torque can also be defined as the change of total magnetic energy of system with reference to rotor revolution when no primary stator current is present. In most of the cases, the cogging torque is computed from the change in the magnetic co-energy in air gap and the slot as the rotor advances by a small angle [Ackermann *et al.* 1992, Bianchi *et al.* 2002, Breton *et al.* 2000]. However, when calculating torque by this method, an important and difficult part is to compute the tangential component of air gap flux density. The tangential component may have less contribution in the air gap flux density while its rate of change of energy with rotor position may be large.

Due to these difficulties, alternate method to compute cogging torque in PM machine has been suggested by Zhu which includes summing of the lateral magnetic forces along the stator tooth sides [Zhu *et al.*, 1992]. Zhu simplified the calculation of cogging torque in three steps; (i) Determination of the air gap flux density considering

slotless stator (ii) Including relative permeance factor due to presence of slots and (iii) Computation of the cogging torque using modified air gap flux density with relative permeance at different rotor positions.

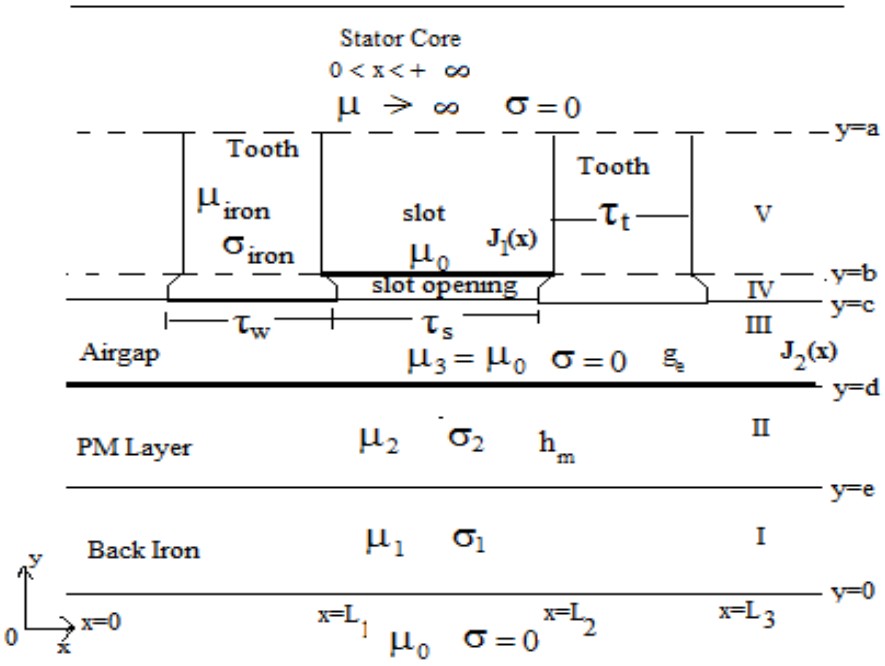

Fig. 2.9 Analytical Model for calculating cogging torque

Conformal Mapping [Lin *et al.* 2012] and quasi 3-D modeling of cogging torque in AFPM machines [Tiegna *et al.* 2014] has also been reported for computation of cogging torque. The approach suggested by author has been extended and in present case, the cogging torque is calculated as the sum of torque produced in three different regions [Zhu *et al.* 1992]. The analytical model for computation of cogging torque is shown in Fig. 2.9. Since, cogging torque is calculated when the primary winding current is absent. In the proposed method, the flux is calculated at three different regions from $0<x<L_1$, $L_1<x<L_2$ and $L_2<x<L_3$ separately when J_1 is zero.

Flux Density can be calculated in the same manner as the total torque.

$$\tilde{\mathbf{B}}_{3y}(\xi,c)=\nabla\times\mathbf{A}_{3z}=-j\xi\tilde{\mathbf{A}}_{3z}(\xi,c) \tag{2.89}$$

$$B_{3y}(x,c)=jk\mu_3 J_p\frac{W(-k,c)}{K(-k)}\exp(-jkx) \tag{2.90}$$

The torque with J_1 is zero, equation (2.72) becomes,

$$T=0.5Dp\int_0^L \Re e\left[\tilde{\mathbf{J}}_2^*(\xi)\mathbf{B}_{3y}\right]dx \tag{2.91}$$

The summation of three torques with J_1 absent in slots gives the total cogging torque w.r.t. rotor position.

2.7 Conclusions

In this chapter, a new analytical method has been proposed for the analysis of SMPM motor. The method is based on the solution of governing field equations using Spatial Fourier Transform. The primary winding current and PM are represented by their equivalent current sheets. The calculation of magnetic field and torque using Residue Theorem and Parseval's Theorem has been explained in detail. The back-EMF and cogging torque calculation by proposed method has also been discussed. The application of proposed analytical method has been extended for the performance analysis of AFPM motors. The next chapter discusses the fabrication and operation of the SMPM motors developed for the validation of the proposed analytical method. Different configurations of the SMPM machine like radial flux and axial flux have been fabricated and their operational features have been highlighted.